Instantaneous normal modes, resonances, and decay channels in the vibrational relaxation of the amide I mode of *N*-methylacetamide-D in liquid deuterated water

Adolfo Bastida,[1,a)] Miguel Angel Soler,[1] José Zúñiga,[1] Alberto Requena,[1] Adrián Kalstein,[2] and Sebastián Fernández-Alberti[2]
[1]*Departamento de Química Física, Universidad de Murcia, Murcia 30100, Spain*
[2]*Universidad Nacional de Quilmes, Roque Saenz Peña 352, Bernal B1876BXD, Argentina*

(Received 4 March 2010; accepted 5 May 2010; published online 8 June 2010)

A nonequilibrium molecular dynamics (MD) study of the vibrational relaxation of the amide I mode of deuterated *N*-methylacetamide (NMAD) in aqueous (D_2O) solution is carried out using instantaneous normal modes (INMs). The identification of the INMs as they evolve over time, which is necessary to analyze the energy fluxes, is made by using a novel algorithm which allows us to assign unequivocally each INM to an individual equilibrium normal mode (ENM) or to a group of ENMs during the MD simulations. The time evolution of the energy stored in each INM is monitored and the occurrence of resonances during the relaxation process is then investigated. The decay of the amide I mode, initially excited with one vibrational quantum, is confirmed to fit well to a biexponential function, implying that the relaxation process involves at least two mechanisms with different rate constants. By freezing the internal motions of the solvent, it is shown that the intermolecular vibration-vibration channel to the bending modes of the solvent is closed. The INM analysis reveals then the existence of a major and faster decay channel, which corresponds to an intramolecular vibrational redistribution process and a minor, and slower, decay channel which involves the participation of the librational motions of the solvent. The faster relaxation pathway can be rationalized in turn using a sequential kinetic mechanism of the type $P \rightarrow M+L \rightarrow L$, where P (*parent*) is the initially excited amide I mode, and M (*medium*) and L (*low*) are specific midrange and lower-frequency NMAD vibrational modes, respectively. © *2010 American Institute of Physics*.
[doi:10.1063/1.3435212]

I. INTRODUCTION

During the past decade great advances have been made in the time-resolved infrared and Raman spectroscopic techniques,[1–12] which made it possible to monitor the vibrational energy flows occurring within small organic molecules in aqueous solution on a time scale of several hundred femtoseconds.[13] A significant number of these studies focused on compounds with peptide bonds. Ultimate understanding of the structural-dynamics-function relationship in proteins requires a detailed knowledge of the energy flow within these molecules. In this respect, vibrational energy relaxation and intramolecular vibrational energy redistribution are fundamental processes associated with the biological function of a large variety of proteins.[14–17] The excitation of the amide I mode of a peptide group in particular has been proposed as the first step in the function of ATP-binding proteins.[18] The energy released by the vibrational relaxation of the amide I mode can be used by the α-helix to change its conformation.

The amide groups play an important role in the stabilization of a protein fold due to their participation in both the intramolecular backbone and solvent-protein hydrogen bondings. The vibrational frequency of the amide I mode, which mainly involves the stretching of the peptide C═O bond, is sensitive to the three-dimensional structure of the protein[4] and can therefore be used as a probe to determine the conformational dynamics of the molecule in solution.[19–21] The advent of two-dimensional infrared spectroscopy has in this sense provided a new source of reliable experimental data for the elucidation of the conformations of peptide building blocks. In addition, some experimental[12,22] and theoretical[23,24] studies have recently analyzed the energy transport through biomolecular systems, considering different excitation techniques (UV or IR excitations, temperature jump, etc.).

Following the pioneering experimental work by Hochstrasser and Hamm,[4] different ultrafast pump probe spectroscopic techniques have been used to study a wide variety of molecules with peptide bonds including *N*-methylacetamide (NMA), small peptides, and large proteins.[4,19,25] Although, in principle, different relaxation dynamics of the amide group are expected, depending on their exposure to the solvent and the conformations of the peptide, experiments show[4] that the decay time of the amide I mode is close to 1 ps for all systems considered. This finding reveals in some way a general intrinsic behavior of the peptide group in any kind of environment. Accordingly, the comparatively simple NMA molecule has become a suitable model to investigate the

a)Electronic mail: bastida@um.es.

spectroscopy of the peptide bond, as evidenced by the large number of experimental[4,10,6,26–29] and theoretical[27,30–38] studies reporting on this system.

Although in most cases the vibrational decay of the amide I mode measured in pump probe experiments fits well to a single-exponential function,[4,19,25] a pronounced biexponential decay was reported by Hostraesser *et al.*[4,6] for deuterated *N*-methylacetamide (NMAD) in aqueous D_2O solution. Even in this case, the signal is dominated by the fast decay component (0.45 ps), with the slow decay component (4 ps) having an amplitude of only ca. 20% of the total signal. The biexponential decay of the amide I mode of NMAD has been confirmed experimentally more recently by Tokmakoff *et al.*[28] with shorter relaxation times for each component (0.20 and 0.86 ps, respectively). These experimental findings indicate that the process certainly involves at least two relaxation mechanisms with different rate constants. Accordingly, the intramolecular energy redistribution (IVR) of the amide I mode into normal modes with lower frequencies is expected to play a key role in the vibrational relaxation of the amide I mode. In this line, it is worth noting the previous study by Fujisaki and Straub[39] on the vibrational relaxation of amide I modes in cytochrome *c* solvated with water using time-dependent perturbation theory. These authors concluded that there are protein-mediated and water-mediated pathways, depending on which residue is excited.

From the theoretical point of view, an adequate molecular dynamics (MD) simulation of a vibrational energy relaxation process requires first the use of accurate models for the potential energy surfaces of the molecules involved in the process. In this sense, a number of *ab initio* based potential energy functions for NMA have recently been developed at different levels of theory.[30,36,38,40,41] These potentials are expected to provide in principle a better description of relaxation dynamics of the amide I mode in solution than the standard biophysical force fields such as AMBER,[42] CHARMM,[43] GROMOS,[44] and OPLS.[45] Comparison of the vibrational frequencies calculated for different force fields shows, however, that the accuracy of the *ab initio* over the empirical force fields is not uniform for all modes. In addition, since the experimental evidence reveals the universal character of the amide I vibrational relaxation, thus favoring the use of a generic force field suitable for different molecular systems containing the amide group, and since most of the previous theoretical descriptions of the NMA relaxation in water solution have been carried out using standard empirical potentials,[31,35,37] we also assumed the use of these potentials in this work.

The theoretical approach most widely used to describe the dynamics of vibrational relaxation processes is Fermi's golden rule with classical force-force correlation functions.[7,46–50] For the vibrational relaxation of NMAD in D_2O, however, this method gives a decay time about two orders of magnitude larger than the experiment.[31] More accurate results for this system are obtained by using time-dependent perturbation theory, which accounts for the effects of the nonhomogeneous environment in a more realistic way.[35] This method has been improved by including the fluctuations of the parameters in the Hamiltonian within the vibrational adiabatic approximation.[37] The time-dependent normal mode frequencies along the MD trajectories are obtained in this case from structures of NMA that are partially optimized with fixed solvent molecules. Thus, the dominant relaxation pathways are characterized by introducing path-specific decay times. According to all these time-dependent studies, the relaxation of the amide I mode is essentially an IVR process with little contribution from the solvent molecules, in which fast energy transfer from the amide I mode to the lower-frequency modes of NMAD is mediated by Fermi resonances. A very recent application of this methodology to NMAD/$(D_2O)_n$ $(n=0–3)$ clusters provided, however, results which indicate that the amide II mode is the main energy acceptor of the excited amide I mode, with an important role played by the water molecules in the relaxation mechanisms.[51] Nevertheless, these time-dependent methods are limited to the study of the short-time decay of the amide I mode, so they are not useful in analyzing the long-time contributions to the vibrational relaxation observed experimentally.

Direct simulations of the vibrational relaxation process can alternatively be performed by nonequilibrium MD.[52–54] This method has been used by Nguyen and Stock[31] to study the amide I vibrational relaxation of NMAD in D_2O, employing a quasiclassical sampling of the initial conditions to mimic the initially excited system in combination with an instantaneous normal modes (INMs) analysis.[55–57] By application to this system, these authors established the validity and the performance of the methodology proposed and confirmed the biexponential nature of the amide I energy relaxation. However the use of nonequilibrium MD plus INMs analysis to monitor the intramolecular flow of energy among the vibrational modes and thus elucidate the details of the relaxation mechanism requires, in addition, a practical and efficient way of assigning the INMs as they evolve over time. It is known that the coupling between the amide I and the HOH bending modes of the water solvent molecules is responsible for the splitting into two peaks of the amide I band of NMA in neat H_2O.[58,59] For deuterated water, the frequency of the DOD bending mode is however too low to directly perturb the amide I band, so it is not clear to what extent this mode affects the vibrational relaxation process. The main pathways of IVR in solvated NMAD after amide I excitation remain in this sense to be analyzed by MD simulations.

The aim of this paper is therefore to address the vibrational energy relaxation of the amide I mode of the NMA in aqueous solution (D_2O) and the subsequent intramolecular vibrational redistribution of the energy, using nonequilibrium MD simulations. For this purpose, we use equilibrium normal modes (ENMs) of the NMAD to propagate the normal coordinates, instead of Cartesian coordinates, and INMs to analyze the results extracted from the nonequilibrium simulations. A new method is proposed which enables us to assign "on the fly" each ENM to an individual INM or to a set of INMs during the MD simulations, thus facilitating to a large extent the analysis of the energy stored in each vibrational mode. This procedure also allows us to investigate the presence of resonances in the energy pathways and to follow

the time evolution of the energy flow. Direct use of ENM coordinates to solve the equations of motion in addition permits constraints to be applied to the motion of the system in a straightforward way. The paper is organized as follows. In Sec. II we present the methodological aspects of the MD simulations using ENMs coordinates, the way in which the instantaneous normal mode analysis is carried out, including the algorithm proposed to assign these modes to the ENMs, and the computational details. Section III is devoted to the discussion of the simulations results, especially those concerning the main pathways of IVR, and finally a summary and the conclusions are given in Sec. IV.

II. METHODOLOGY

A. MD coordinates

In order to carry out the nonequilibrium MD simulations of the NMAD/$D_2O_{(l)}$ system we express the total energy as a sum of three terms as follows:

$$E_{\mathrm{tot}} = E_{\mathrm{NMAD}} + E_{\mathrm{D_2O_{(l)}}} + V_{\mathrm{NMAD/D_2O_{(l)}}}. \tag{1}$$

The term E_{NMAD} contains all the contributions depending exclusively on the coordinates of the solute NMAD molecule, including the molecular center of mass vector $\boldsymbol{R}_{\mathrm{CM}}$, the quaternions $\boldsymbol{q}=q_1,q_2,,q_3,q_4$ that specify the rotation of the molecule,[52] and the ENMs $Q_i^{\mathrm{e}}, i=1,\ldots,N=30$ that describe its vibrational motions. We use this set of coordinates $\{\boldsymbol{R}_{\mathrm{CM}},\boldsymbol{q},Q_i^{\mathrm{e}}\}$, instead of the Cartesian coordinates usually employed in MD simulations because they are more closely related to the usual partition of the energy as the sum of the translation, rotation, and vibration contributions, that is,

$$E_{\mathrm{NMAD}} = E_{\mathrm{NMAD}}^{\mathrm{trans}} + E_{\mathrm{NMAD}}^{\mathrm{rot}} + E_{\mathrm{NMAD}}^{\mathrm{vib}}. \tag{2}$$

The translational energy in this expression is given by

$$E_{\mathrm{NMAD}}^{\mathrm{trans}} = \frac{\boldsymbol{P}_{\mathrm{CM}}^2}{2M_{\mathrm{NMAD}}}, \tag{3}$$

where $\boldsymbol{P}_{\mathrm{CM}}$ is the center of mass momentum and M_{NMAD} is the total mass of the molecule. The rotational energy is written in terms of the moments of inertia matrix $\boldsymbol{I}$ and the angular velocity $\boldsymbol{\omega}$ in the usual way,

$$E_{\mathrm{NMAD}}^{\mathrm{rot}} = \tfrac{1}{2}\boldsymbol{\omega I \omega} \tag{4}$$

and the vibrational energy is given in terms of the ENMs Q_i^{e} by

$$E_{\mathrm{NMAD}}^{\mathrm{vib}} = \frac{1}{2}\sum_{i=1}^{N} (\dot{Q}_i^{\mathrm{e}})^2 + V_{\mathrm{NMAD}}(Q_i^{\mathrm{e}}), \tag{5}$$

where N is the number of vibrational degrees of freedom of the NMAD molecule and $V_{\mathrm{NMAD}}(Q_i^{\mathrm{e}})$ is the intramolecular potential energy function. The use of the normal modes as propagation coordinates in addition allows us to carry out simulations straightforwardly with some normal modes frozen, which are required to analyze the different relaxation pathways of the system, as shown in Sec. III below. Also note in Eq. (2) that we neglected the rotational-vibrational couplings, and therefore assumed that the NMAD molecule rotates as a rigid rotor. In order to check this approximation, we calculated the instantaneous moments of inertia related to the principle axes during a typical trajectory and found that they deviate by less than 3% from their equilibrium values, which validates the rigid rotor model employed.

The term $E_{\mathrm{D_2O_{(l)}}}$ in Eq. (1) accounts for the energy of the solvent. As shown below, the vibrational motions of the water molecules do not play an essential role in the relaxation process, so they are described using the Cartesian coordinates for the sake of computational simplicity. The last term in Eq. (1), $V_{\mathrm{NMAD/D_2O_{(l)}}}$, is the intermolecular potential energy that couples the motions of the solute and the solvent.

B. Instantaneous normal modes analysis

The ENMs Q_i^{e} provide a decoupled description of the vibrational motions of the solute NMAD molecule up to second order at the equilibrium geometry. During the relaxation of the initially excited amide I mode, the molecule of solute may explore regions of the phase space which are far away from the equilibrium geometry due to its proper thermal motion, to the energy fluxes originated in the relaxation and to the intermolecular interactions with the solvent molecules. The couplings between the ENMs are then enhanced, making it eventually difficult to quantify the energy stored in each individual normal mode. A convenient way of tackling this problem is to use the INMs, to analyze the dynamics of the system.[55–57] These modes are defined as the vibrational coordinates which diagonalize the Hessian matrix at a given configuration of the molecule, and they accordingly provide an instantaneous decoupled second-order description of the vibrational motions of the molecule at the corresponding time-dependent configuration.

In order to use the INMs it is convenient to define them in terms of the ENMs. This can be done by first expanding the sum of the V_{NMAD} and $V_{\mathrm{NMAD/D_2O_{(l)}}}$ potentials in a power series of the ENMs about the configuration of the molecule at a given time t_0 as follows:

$$V = V(Q_i^{\mathrm{e}}(t_0)) + \sum_{i=1}^{N} K_i(Q_i^{\mathrm{e}} - Q_i^{\mathrm{e}}(t_0)) + \frac{1}{2}\sum_{i=1}^{N}\sum_{j=1}^{N} K_{ij}(Q_i^{\mathrm{e}} - Q_i^{\mathrm{e}}(t_0))(Q_j^{\mathrm{e}} - Q_j^{\mathrm{e}}(t_0)) + \cdots, \tag{6}$$

where K_i and K_{ij} are the corresponding linear and quadratic force constant, and second by diagonalizing the resulting Hessian matrix $\boldsymbol{K}$,

$$\boldsymbol{L}^{\dagger}\boldsymbol{K}\boldsymbol{L} = \boldsymbol{\lambda}, \tag{7}$$

to obtain the vibrational frequencies, $\nu_i = \sqrt{\lambda_i}/2\pi$, of the INMs, and the eigenvector matrix, $\boldsymbol{L}$, which relates the INMs with the ENMs as follows:

$$Q_i^{\mathrm{INM}} = \sum_{j=1}^{N} l_{ji}(Q_j^{\mathrm{e}} - Q_j^{\mathrm{e}}(t_0)). \tag{8}$$

Since the $\boldsymbol{L}$ matrix is orthonormal, we can conversely express the ENMs in terms of the INMs,

$$Q_j^e = \sum_{i=1}^{N} l_{ji} Q_i^{INM} + Q_j^e(t_0). \tag{9}$$

By substitution of this expression into Eq. (6) we can write the potential energy function V in terms of the INMs as

$$V = V_0 + \frac{1}{2}\sum_{i=1}^{N} \lambda_i (Q_i^{INM} + a_i)^2 + \cdots, \tag{10}$$

where a_i are the coordinate shifts given by

$$a_i = \frac{1}{\lambda_i}\sum_{j=1}^{N} K_j l_{ji}, \tag{11}$$

and V_0 is the shift-corrected equilibrium potential,

$$V_0 = V(Q_i^e(t_0)) - \frac{1}{2}\sum_{i=1}^{N} \lambda_i a_i^2. \tag{12}$$

Also it can be easily shown that the vibrational kinetic energy transforms in terms of the INM momenta as

$$T^{vib} = \frac{1}{2}\sum_{i=1}^{N} (\dot{Q}_i^e)^2 = \frac{1}{2}\sum_{i=1}^{N} (\dot{Q}_i^{INM})^2. \tag{13}$$

By neglecting the third and higher order terms in the potential energy function, we can write the vibrational energy of each INM as

$$E_i^{INM} = \tfrac{1}{2}(\dot{Q}_i^{INM})^2 + \tfrac{1}{2}\lambda_i (Q_i^{INM} + a_i)^2 \tag{14}$$

so the total vibrational energy of the solute is approximated by

$$E_{NMAD}^{vib} = V_0 + \sum_{i=1}^{N} E_i^{INM}. \tag{15}$$

The accuracy of this expression in accounting for the exact vibrational energy given by Eq. (5) is verified in Sec. III below.

Let us consider now the INMs of the NMAD molecule. In Table I we include the time averaged frequencies of these modes, with their standard deviations, as calculated from the MD simulations described in Sec. III by sorting the time-dependent frequencies in increasing order. As may occur,[60] for the first three modes we found trajectories with negative force constants λ_i which give imaginary frequencies. When averaged, only the vibrational frequency of the first mode remains imaginary and, as is usually done,[55–57] we take its value as negative. It is also observed in Table I that the standard deviations of the INM frequencies vary appreciably but for most of the modes the difference between two successive frequencies is smaller than the sum of their standard deviations.

The fact that the vibrational energy of the solute could be expressed as the sum of the individual INM contributions, as given in Eq. (15), is crucial since it allows us to calculate the amount of energy which is stored in each mode during the relaxation process. The problem with this lies in the identification of INMs as they evolve over time since they may mix and cross when their time-dependent frequencies become close enough. Previous work[61] has shown that sorting the INMs by increasing frequencies is anything but useful in this respect. We should note that a similar problem was found by Kidera *et al.*[62] in their analysis of results of MD simulations based on the definition of a set of normal mode coordinates at each time instant of the trajectory by principal component analysis.[62,63] As the authors indicate,[62] there is a difficulty in the definition of the correspondence when two or more modes are in the resonance condition. In such a resonance case, correspondence of the modes at different times cannot be defined.

TABLE I. Time averaged vibrational frequencies (in cm^{-1}) of the INMs of the NMAD molecule including their standard deviations.

Order	Frequency
1[a]	−227.1 ± 228.2
2[a]	55.6 ± 204.5
3[a]	234.5 ± 100.0
4	335.1 ± 59.7
5	431.5 ± 59.7
6	510.2 ± 49.7
7	592.9 ± 14.3
8	649.9 ± 36.8
9	776.6 ± 22.7
10	832.8 ± 27.9
11	961.4 ± 46.0
12	1015.8 ± 35.1
13	1057.7 ± 29.0
14	1094.7 ± 27.3
15	1139.1 ± 30.7
16	1339.3 ± 31.0
17	1376.0 ± 25.0
18	1402.0 ± 23.3
19	1427.8 ± 22.4
20	1457.0 ± 21.0
21	1540.0 ± 32.2
22	1616.5 ± 21.5
23	1691.9 ± 8.1
24	2432.5 ± 7.1
25	2810.1 ± 32.9
26	2875.9 ± 7.5
27	2969.4 ± 6.4
28	2979.1 ± 5.8
29	2989.6 ± 6.4
30	3002.5 ± 14.2

[a]Imaginary frequencies are given as negative frequencies.

We propose the use of the ENM as templates to track the identity of the INMs over time. Accordingly, the INMs can be classified as pure or mixed, depending on the contributions of the ENM. In a pure INM, one of the elements of the lineal combination (8) is dominant so the INM is quite similar to the corresponding ENM. A mixed INM includes, however, significant contributions from different ENMs. The pure INMs are easy to identify at any time during the simulation and correspond to well-defined motions of the molecule associated to the dominant ENM. In contrast, the mixed INMs are difficult to identify due to the changes with time of the sparse ENM contributions. These modes sometimes appear as groups of modes which exchange the contributions of a given number of ENMs, displaying complicated motions of the molecule.

TABLE II. Time averaged values of the highest contributions of the ENMs to the INMs of the NMAD molecule. The first data set given in columns two and three is obtained by sorting the INMs by increasing frequencies, and the second data set given in column four is obtained using the min-cost algorithm to assign the INMs in terms of the ENMs.

	Frequency ordering		Min-cost assignment	
INM	Max overlap	ENM	Max overlap	Label[a]
1	0.21	2	0.57	$\tau(CH_3)$
2	0.37	3	0.59	$\tau(CH_3)$
3	0.30	3	0.71	τ(CN)
4	0.48	4	0.78	δ(CNC)
5	0.55	5	0.85	δ(CCN)
6	0.42	6	0.72	Amide V
7	0.75	7	0.84	Amide IV
8	0.55	8	0.58	Amide VI
9	0.75	9	0.76	ν(CC)
10	0.67	10	0.68	Amide III
11	0.14	11	0.39	$r\parallel(CH_3)C$
12	0.15	11	0.36	$r\perp(CH_3)N$
13	0.14	13	0.32	$r\parallel(CH_3)N$
14	0.17	15	0.35	$r\perp(CH_3)C$
15	0.23	15	0.38	ν(CN)
16	0.14	16	0.31	$\delta_s(CH_3)C$
17	0.10	16	0.42	$\delta_a(CH_3)N$
18	0.10	16	0.35	$\delta_s(CH_3)C$
19	0.10	16	0.27	$\delta_s(CH_3)N$
20	0.14	16	0.41	$\delta_a(CH_3)C$
21	0.51	21	0.52	$\delta_s(CH_3)N$
22	0.71	22	0.72	Amide II
23	0.91	23	0.91	Amide I
24	0.98	24	0.98	Amide A
25	0.27	02	0.56	$\nu_s(CH_3)C$
26	0.23	25	0.54	$\nu_s(CH_3)N$
27	0.12	27	0.43	$\nu_a(CH_3)N$
28	0.12	30	0.43	$\nu_s(CH_3)N$
29	0.11	28	0.42	$\nu_a(CH_3)C$
30	0.13	30	0.44	$\nu_s(CH_3)C$
Average	0.35		0.55	

[a]From Ref. 68. τ is the torsion, δ is the bending, ν is the stretching, r is the rocking, a is asymmetric, and s is symmetric.

One way of quantifying the pure or mixed character of an INM is to analyze the l_{ij}^2 values which, according to Eq. (8), measure the weight of the ith ENM to the jth INM. In the second column of Table II we give the time averaged values of the highest l_{ij}^2 contributions of the ENMs to the INMs, as selected again sorting as the INMs by increasing frequencies. As observed, some INMs, such as the 23rd and 24th which correspond to the amide I and the amide A modes, respectively, have a very pure character since the overlap with the corresponding ENM exceeds 90%. These modes in turn have well-defined frequencies (see Table I). There is also a large number of INMs (about two-thirds of them) for which the highest averaged contribution of a given ENM is smaller than 50%, which is the value used to distinguish between the pure and the mixed INMs. Moreover, for some INMs, the highest contribution comes from the same ENMs, as for modes 16th–20th. It is then quite clear that a realistic assignment of the INMs based exclusively on the frequency ordering criterion becomes impractical.

In order to address this problem, in this work we propose the use of a novel algorithm to assign the INMs in terms of the ENMs. A good assignment in this respect should establish a one-to-one correspondence between both sets of modes through the highest values of the l_{ij}^2 weights. This can be done by selecting those elements of the $\boldsymbol{L}$ matrix, one for each row, and each pertaining to a different column (or vice versa), which maximize the sum of their squared values. This is a well-known problem in Economics known as the min-cost or min-sum assignment problem, which can be efficiently solved using the so-called Hungarian method.[64] We adapted this method to our problem using the code given by Toth *et al.*[64] For a given matrix, this code in fact provides a set of elements, each one belonging to a different row and column, whose sum is minimal. So, in order to maximize the sum of the l_{ij}^2 elements, as required in our case, we apply the code to the matrix formed by the negative values of the l_{ij}^2 elements.

In Table II we also include the results obtained from the application of the min-cost algorithm to assign the INMs. Apart from giving a one-to-one relationship between the two sets of normal modes, the min-cost algorithm provides, in general, higher values for the l_{ij}^2 elements selected than the frequency ordering method, with more than half of the INMs having maximum overlaps with the corresponding ENMs higher than 50%. In spite of this improvement, there remain groups of mixed INMs which cannot be unambiguously assigned to a single ENM. We also observed in the simulations that the ENM contributions to these unassigned INMs fluctuate quite a lot with time. The 11th–20th groups of INMs, in particular, hereafter referred to as group a of modes, are mainly formed by combinations of rocking and bending methyl ENMs and a backbone ENM mode, which suppose an overall contribution to the INMs of about 70%. The 27th–30th groups of INMs, hereafter referred to as group b of modes, are made up of more energetic stretching methyl ENMs accounting for a total contribution of 55%. Interestingly, the b modes also have a significant contribution, ~40%, from the dominant ENMs of group a, and the a modes have a non-negligible contribution, ~15%, from the dominant ENMs of group b. Both groups therefore share some ENM character which allows the transfer of energy between them, as will be discussed in Sec. III.

C. Computational details

We performed the MD simulations by placing the NMAD molecule in a cubic box of 1.975 nm length containing 251 D_2O molecules to reproduce the experimental density[65] (ρ=1.104 36 g/cm^3) with periodic boundary conditions. Subroutines of the TINKER modeling package[66] have been used in our code to evaluate the forces and the potential energy function. The AMBER force field[42] has been employed to model the solute NMAD ($H_3C-COND-CH_3$) and the flexible TIP3P water model[43] with doubled hydrogen masses included in the CHARM force field (see below) to model the D_2O solvent. The equations of motion were integrated by using the leap-frog algorithm with a time step of 0.5 fs. For the rigid body rotational motion of the solute NMAD mol-

ecule, we used the midstep implicit leap-frog rotational algorithm proposed by Svanberg.[67] A cutoff of 10 Å was applied for the nonbonded interaction calculations.

The ENMs were obtained from the optimized geometry of the *trans*-cc-NMA conformer, which is the most stable as calculated using the AMBER force field, and provides normal modes frequencies which are in good agreement with previously reported values.[30,68,69] The initial coordinates for the vibrational relaxation dynamics were taken from 16 previous MD simulations of 1250 ps at 300 K, which were started using random velocities. An initial period of time of 750 ps was used to equilibrate the system, collecting data at 20 ps intervals in the last 500 ps. During the simulations the temperature was maintained at a mean value of 300 K by coupling to a thermal bath[70] with a time constant of 0.1 ps. Thus, 400 sets of initial positions and momenta were stored for subsequent nonequilibrium vibrational relaxation simulations.

The simulations of the relaxation process were performed in the *NVE* ensemble in order to avoid any influence of the velocity scaling on the results. Accordingly, 400 trajectories of 40 ps were propagated in order to obtain reasonable statistics for all the quantities reported. At $t=0$, an excess of energy of one vibrational quantum was suddenly deposited in the NMAD molecule by displacing the amide I mode until its energy reached the proper value [see Eq. (14)]. Finally, Eq. (9) was used to obtain the initial values of the ENMs.

III. NUMERICAL RESULTS AND DISCUSSION

A. Vibrational relaxation of the NMAD molecule

We investigated first the validity of Eq. (15) to calculate the vibrational energy of the NMAD molecule as a sum of individual contributions of the INMs. These contributions are given by Eq. (14) and their values depend on the a_i shifts, which are in turn inversely proportional to the harmonic force constants λ_i [Eq. (11)]. As a consequence, large numerical uncertainties are expected when any λ_i comes close to zero, which is quite frequent for some of the lowest frequency modes. Since the kinetic energy is free from singularities of this type, we avoided this numerical problem by using the virial theorem, $E^{\mathrm{vib}}=2T^{\mathrm{vib}}$, to calculate the vibrational energy of the INMs, We previously verified that the virial theorem accurately applies to the medium and high frequency modes and then we used this theorem to calculate the energies of the remaining modes.

In Fig. 1 we plot the total vibrational energy of the NMAD molecule as a function of time calculated using both Eq. (5) in terms of the ENMs, which is exact, and Eq. (15) in terms of the INMs but using the virial theorem for the three lower-frequency modes. As seen, the agreement between both results is excellent, which validates the use of the INMs for analyzing the relaxation pathways. Both decay curves are well reproduced by a single-exponential function as follows:

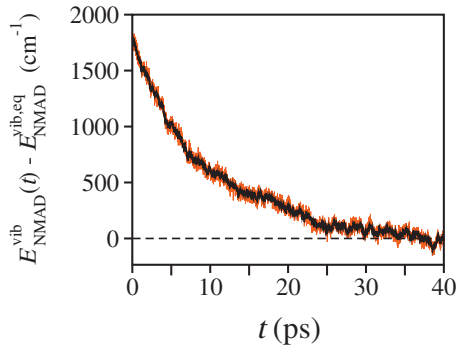

FIG. 1. Vibrational energy of the solute NMAD molecule relative to its equilibrium value as calculated using Eq. (5) in terms of the ENMs (black line) and the virial theorem (red line) with the kinetic energy of the INMs given by Eq. (13).

$$\frac{E^{\mathrm{vib}}_{\mathrm{NMAD}}(t)-E^{\mathrm{vib,eq}}_{\mathrm{NMAD}}}{E^{\mathrm{vib}}_{\mathrm{NMAD}}(0)-E^{\mathrm{vib,eq}}_{\mathrm{NMAD}}}=e^{-t/\tau}, \tag{16}$$

where the superscript eq stands for the equilibrium value of the NMAD vibrational energy. The calculated relaxation time is $\tau=9.6$ ps. This value is about twice that measured by Dlott *et al.*[29] in their recent ultrafast infrared-Raman spectroscopy study of the relaxation of the $\nu_s(CH_3)$ mode of NMAD in $D_2O_{(l)}$. It is difficult to assert whether the difference between the experimental and the simulated relaxation times of the NMAD molecule is exclusively due to the fact that the initially excited modes are different. Nevertheless, we note that the time scale of the relaxation of the vibrational energy of the molecule provided by our simulations is similar to the experimental one. To reinforce this point, we refer to a recent MD study carried out by Stock *et al.*[71] on photoinduced heat transfer from the NMA molecule in various solvents. In this study, the resulting NMA cooling curve in water is well reproduced by a biexponential function, with decay times of 0.07 ps (20%) and 7.7 ps (80%). Interestingly, the largest decay time, which dominates the curve at the energy range relevant to our study, is comparable to the relaxation time derived from our analysis, despite the excitation method (a temperature jump) and the amount of energy stored (the molecule is heated up to 500 K) being different from those used in the present simulations.

B. Relaxation time of the amide I mode

The next issue that we addressed concerns the participation of the solvent in the relaxation of the amide I mode. The time averaged frequency of the amide I mode is 1692 cm^{-1} (see Table I), so, in principle, it should be possible to transfer part of the energy initially acquired by this mode through an intermolecular vibration-to-vibration (VV) mechanism, to the bending modes of the deuterated water molecules of the solvent, which have a measured frequency[72] of $\omega_b=1209.4$ cm^{-1}, and to deposit the spare energy in the water librational modes, which are centered[73] at $L_1=315$ and $L_2=520$ cm^{-1} with bandwidths around 100 cm^{-1}. In order to check this, it is important to use a realistic flexible model for the solvent D_2O molecules. The TIP3P model included in the

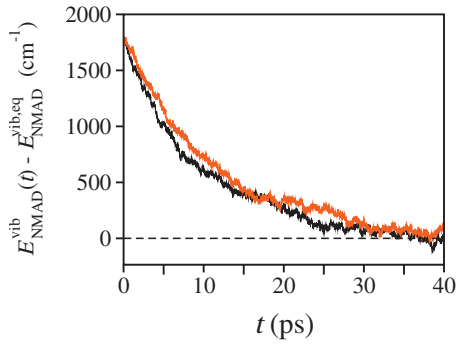

FIG. 2. Vibrational energy of the solute NMAD molecule relative its equilibrium value as calculated using flexible (black line) and frozen (red line) models for the D_2O solvent molecules.

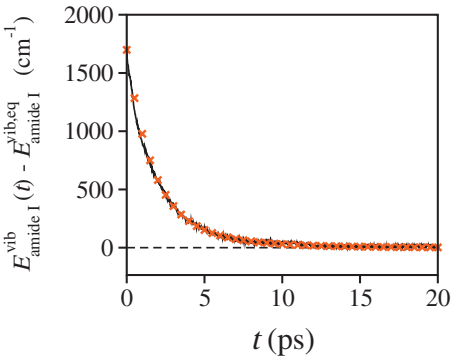

FIG. 3. Vibrational energy of the amide I INM of NMAD relative to its equilibrium value (black line). Red crosses are the biexponential fit with amplitudes $c_1=0.80$ and $c_2=0.20$.

CHARMM force field[43] and used in this work gives, in this sense, a bending normal mode frequency ω_b of 1264.7 cm^{-1}, which is quite similar to the experimental value. We should note also that the stretching frequencies measured for the D_2O solvent molecules,[72] $\omega_b=2500-2600$ cm^{-1}, are too high for these modes to be excited when the amide I mode is relaxed. In order to check whether the intermolecular bending VV relaxation channel is open, we carried out an independent set of simulations freezing the internal motions of the D_2O molecules by using of the SHAKE algorithm,[74] thus impeding the VV transfer of energy. In Fig. 2 we compare the vibrational decay curves of the NMAD molecule obtained with and without SHAKE. As observed, the two decay curves are very similar. The relaxation time obtained for the SHAKE curve, 9.7 ps, is practically the same as that calculated using the flexible solvent model, 9.6 ps, which demonstrates that the vibrational relaxation of the amide I mode does not proceed through a VV direct intermolecular transfer process.

Let us consider now more specifically the relaxation of the amide I mode. In Fig. 3 we plot the variation with time of the vibrational energy of the amide I mode, as extracted from the MD simulations. In agreement with previous experimental data[4,6,10] and theoretical results,[28,31,37] we verify first that the decay curve is well reproduced by a biexponential function as follows:

$$\frac{E^{vib}_{amideI}(t) - E^{vib,eq}_{amideI}}{E^{vib}_{amideI}(0) - E^{vib,eq}_{amideI}} = c_1 e^{-t/\tau_1} + c_2 e^{-t/\tau_2}, \tag{17}$$

where c_1 and c_2 are the exponential amplitudes which satisfy $c_1+c_2=1$. In Table III we present the results for the fits together with those from previous theoretical calculations[31,37] and from experiment.[4,28] In order to reduce the uncertainties derived from the use of three fitting parameters in Eq. (17), we set the values of the amplitudes c_1 and c_2 equal to the experimental values obtained both by Hochstrasser *et al.*[4] (0.8, 0.2) and by Tokmakoff *et al.*[28] (0.55,0.45), and fitted

TABLE III. Vibrational relaxation times of the amide I mode (in picosecond) obtained from mono- and biexponential decays [see Eqs. (16) and (17)].

			$\tau_1(c_1)$	$\tau_2(c_2)$	$\bar{T}_1$
Experiment	Hochstrasser *et al.*[a]		0.45 (0.80)	4.00 (0.20)	0.53
	Tokmakoff *et al.*[b]		0.20 (0.55)	0.86 (0.45)	0.31
MD	Present work	Full	1.55 (0.80)	4.01 (0.20)	1.77
			1.24 (0.55)	2.90 (0.45)	1.67
		Solvent SHAKE	1.52 (0.80)	4.26 (0.20)	1.74
		In vacuo	1.41 (0.80)	7.96 (0.20)	1.69
		Q_7^{ENM} frozen	2.10 (0.80)	6.38 (0.20)	2.43
	Nguyen and Stock[c]		1.90 (0.80)	13.3 (0.20)	2.29
Second order perturbation theory[d]			0.43 (1.00)[e]		
			0.60 (1.00)[f]		
			0.54 (1.00)[g]		
			0.93 (1.00)[h]		

[a]Reference 4.
[b]Reference 28.
[c]Reference 31.
[d]Reference 37.
[e]INM with partial energy minimization and inhomogeneous averaging.
[f]INM with partial energy minimization and dynamics averaging.
[g]INM without partial energy minimization and inhomogeneous averaging.
[h]INM without partial energy minimization and dynamics averaging.

only the relaxation times. As observed in Table III, the resulting relaxation times differ significantly, with those obtained using the second set of amplitudes (0.55,0.45) being smaller. The relaxation curves for the two fits are, however, practically indistinguishable, with the (0.8,0.2) fit being slightly more accurate. This shows that special care has to be taken when handling the biexponential relaxation times fitted due to their strong dependence on the amplitudes used. It is more convenient in this respect to use the average relaxation time defined as

$$\bar{T}_1 = \left(\frac{c_1}{\tau_1} + \frac{c_2}{\tau_2} \right)^{-1}, \tag{18}$$

which allows us to characterize the rate of the whole relaxation process in a less ambiguous way. The $\bar{T}_1$ values for the two fits of our simulations, also included in Table III, are, as observed, very similar.

Closer inspection of the relaxation times included in Table III shows first that the times derived by Tokmakoff *et al.*[28] from experiment are substantially lower than those provided by Hochstrasser *et al.*[4] also from experiment, and second that all the relaxation times calculated theoretically from MD simulations are noticeably larger than the experimental ones. Moreover, the relaxation times extracted from our MD simulations are shorter than those provided by Nguyen and Stock,[31] also from MD, with our results being closer to the experimental values. The differences between both sets of MD simulations are more likely to be due to the different force fields used to describe the NMAD/$D_2O_{(l)}$ system than to the use of different assignment methods since the amide I mode is a very pure INM with a contribution of 91% from the corresponding ENM (see Table II). We note also that the larger relaxation time τ_1 obtained from our simulations for the (0.8,0.2) amplitudes agrees quite well with the experimental value, whereas the shorter relaxation time τ_2 is three times longer than the experimental value. The differences between the calculated and experimental relaxation times for the (0.55,0.45) amplitudes are, in turn, larger. In Table III we also include the τ_1 relaxation times recently calculated by Fujisaki and Stock[37] using quantum time-dependent perturbation methods. As observed, these methods provide values for τ_1 in the range of 0.43–0.93 ps which are closer to the experimental values than those extracted from the MD simulations. This means that the fast component of the relaxation curve is better reproduced when the quantum nature of the vibrations is taken into account. Unfortunately, the long tail of the relaxation curve cannot be simulated using these hybrid perturbation methods, which are limited to short times. Overall, our MD-INM simulations are in reasonable agreement with experiment, although the use of a quantum description for the vibrational modes of the NMAD molecule through hybrid quantum/classical time-dependent simulations[75–79] merits further investigation.[80]

C. Relaxation pathways

Let us focus our attention next on the relaxation pathways. The INM assignment method used in this work allows us to follow the energy flows through the INMs during the relaxation process. In Figs. 4–6 we show the evolution of the vibrational energy relative to their equilibrium values for all the assigned INMs. It is observed first that the relaxation process is not statistical, since the energy deposited in each INM varies significantly. The energies of the 1st to 6th, 8th, 25th, and 26th INMs deviate only slightly from their equilibrium values during relaxation. The 7th, 9th, 21st, 22nd, and 24th INMs become some more excited and recover their equilibrium values after elapsed times of 20–30 ps. The modes that receive the largest amounts of energy are the tenth INM, which is associated with the amide III mode, and groups *a* and *b* of INMs, as are clearly observed in Fig. 5.

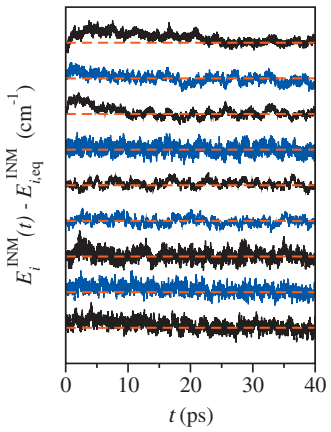

FIG. 4. Vibrational energies of assigned INMs of NMAD relative to their equilibrium values. From bottom to top the plots correspond to the first to ninth INMs. Red dashed lines are the corresponding equilibrium values ($E_{i,eq}^{INM}$=300 K ~ 208.5 cm^{-1}), which are plotted at 100 cm^{-1} intervals.

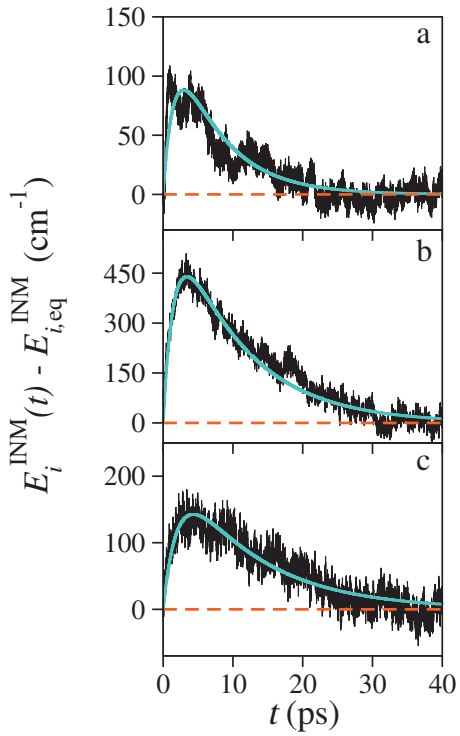

FIG. 5. Vibrational energies of assigned INMs of NMAD relative to their equilibrium values. Plots (a), (b), and (c) correspond to the tenth INM and to the *a* and *b* group of modes, respectively. Black lines are the results from the simulations and blue lines are the fits to Eq. (20).

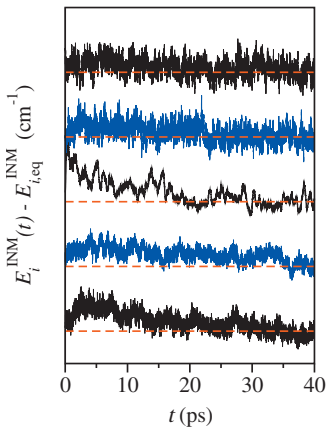

FIG. 6. Vibrational energies of assigned INMs of NMAD relative to their equilibrium values. From bottom to top the plots correspond to the 21st, 22th, 24th, 25th, and 26th INMs. Red dashed lines are the corresponding equilibrium values ($E_{i,eq}^{INM}$=300 K~208.5 cm^{-1}), which are plotted at 100 cm^{-1} intervals.

At first sight, it is surprising how much energy is stored in the group of b modes, which is made up of modes with frequencies higher than that of the amide I mode. The transfer of energy from low to high frequency modes, which does not occur in quantum simulations, has been previously reported in classical dynamics calculations.[38,81–83] In particular, this energy transfer mechanism has recently been described in the vibrational relaxation of the amide II mode of NMA, which transfers its energy to the C—H stretching modes.[38] In this case, the energy flows from the initially excited vibrational mode to a vibrational mode with a frequency double that of the initial mode, even when the initial mode is excited with only a single quantum of vibrational energy. In the present simulations, this unrealistic classical result allows for an amount of 140 cm^{-1} of vibrational energy to be stored in the group of b modes. This amount, which corresponds to ~8% of the energy released by the amide I mode, is equivalent to ~1% population of each of the four modes included in group b. Since the population of the states is the quantity which is directly measured in the experiments, we think that error introduced by the classical description is practically residual. In addition, the energy temporally stored in the group of b modes presumably, in our opinion, comes from the group a for three reasons. First, as previously indicated, the groups a and b of INMs share a significant contributions of ENMs corresponding to motions of the methyl groups. The overlap of vibrational modes has been shown to be directly related to the coupling between them[81,83] since their excitation involves atomic displacements of the same atoms within the molecule. Second, the higher frequency modes of group a could be coupled to the lower-frequency mode of group b through a 1:2 Fermi resonance (see Table I for the corresponding frequencies). Third, the vibrational energy curves of the a and b groups included in Fig. 5 overlap nicely after proper scaling of the energy, as will be shown more explicitly at the end of this section, that is, the excitation and relaxation of the groups a and b of modes occur simultaneously. In quite a similar way, the excitation of the 24th INM, which corresponds to the amide A mode, takes place through a vibrational coupling with the amide I mode. This is in agreement with previous experimental results obtained using 2D femtosecond infrared pump/probe spectroscopy, in which a time-dependent amide A/amide I coupling during vibrational relaxation is reported.[27]

TABLE IV. Main candidates for resonances for the vibrational relaxation of the amide I mode. Overlined variables denote time averaged values and the Δ symbol stands for the standard deviations. All values are in cm^{-1}.

$\alpha+\beta$	$\bar{\omega}_\alpha+\bar{\omega}_\beta$	$\bar{\omega}_\beta\bar{\omega}_{P\alpha\beta}$	$\Delta\omega_{P\alpha\beta}$
7+14	1687.6	4.3	34.6
8+13	1707.6	15.7	53.3
4+17	1711.1	17.4	76.4
10+10	1665.5	26.4	55.1
6+15	1649.3	42.6	64.1
9+11	1738.0	−46.1	55.0

Let us consider now why the energy from the amide I mode flows toward the tenth and group a of INMs. From their recent hybrid perturbation calculations, Fujisaki and Stock[37] suggested that the possible relaxation pathways in this system seem to be driven by simple resonance conditions, so to identify the resonances which could play a role in the relaxation, we calculated the differences between the frequency of the amide I mode, which is the parent (P) mode, and the frequencies of any two other α and β INMs, that is,

$$\omega_{P\alpha\beta}(t) = \omega_P(t) - \omega_\alpha(t) - \omega_\beta(t), \tag{19}$$

and analyzed for which α and β pairs of modes the time averaged values of these differences become closer to zero, $\bar{\omega}_{P\alpha\beta} \approx 0$, which is the resonance condition. The results obtained are given in Table IV. As observed, the best candidates for resonances are the (7,14), (8,13), (4,17), (6,15), and (9,11) pairs of modes, each of them involving one mode of group a, and the (10,10) pair of modes, which accounts for a 2:1 type of resonance. This selection is, in principle, in agreement with the energy profiles previously discussed. However, the lack of excitation of the fourth, sixth, and eighth INMs and the small amount of energy stored in the seventh and ninth INMs (see Fig. 4) seem to cast some doubts about the viability of these energy transfer channels. We should note in this respect that the energy stored in a given INM depends on the excitation rate of that mode, and also on its relaxation rate, that is, on the rate at which the mode transfers its excess energy to other modes. Interestingly, the fourth, sixth, seventh, and eighth modes have frequencies of 335.1, 510.2, 592.9, and 649.9 cm^{-1}, respectively, which overlap quite nicely with those corresponding to the libration bands of liquid deuterated water,[73] which are centered at 315 and 520 cm^{-1} with bandwidths 104 and 124 cm^{-1}. Although these libration frequencies correspond to 0 °C measurements, they vary smoothly with temperature. Accordingly, a fast intermolecular energy transfer between the fourth, sixth, seventh, and eighth INMs of the NMAD and the solvent librations is expected to occur, which would be responsible for the lack of significant excitations in these modes. The frequency of the ninth mode, 776.6 cm^{-1}, is higher than the water librations frequencies, so the lack of

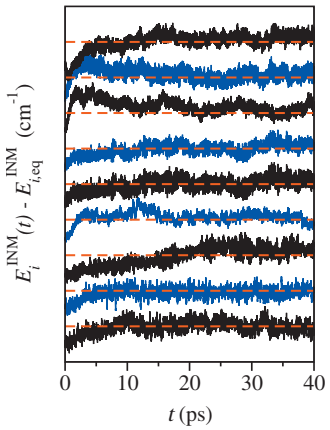

FIG. 7. Vibrational energy of assigned INMs of NMAD relative to their equilibrium values as obtained in simulations carried out in the absence of solvent. From bottom to top the plots correspond to the first to ninth INMs. Red dashed lines are the corresponding equilibrium values ($E_{i,eq}^{INM}$=300 K ~208.5 cm^{-1}), which are placed at 100 cm^{-1} intervals.

excitation in this mode indicates that its participation in the amide I relaxation is very limited, as supported by the fact that this mode provides the most unfavorable resonance condition of those included in Table IV.

The amide I mode could transfer its energy through resonances to the group *a* of modes plus, alternatively, to the water solvent librations instead of to the low-frequency INMs of the solute NMAD molecule. In order to check whether this possibility is feasible, we carried out additional simulations of the amide I relaxation *in vacuo*, that is, in the absence of the solvent, so that the vibrational energy initially deposited in the amide I mode is obliged to redistribute into the remaining INMs of the NMAD solute through pure IVR processes. In these simulations, the final equilibrium energy reached by each mode is 265.3 cm^{-1}, according to an equal distribution of the excess energy in all INMs. The relaxation plots obtained from these simulations for the first nine INMs are shown in Fig. 7. As observed, while the first, second, third, fifth, sixth, and ninth INMs increase their energies monotonically, the fourth, seventh, and eighth INMs now exhibit larger excitations and subsequent relaxations until equilibrium is reached, that is, these three modes preferentially accumulate the energy that cannot be dissipated to the solvent. We should note also that if the relaxation of the amide I mode took place through resonance processes with the direct participation of the solvent librations, the absence the solvent would result in an increase in the global amide I relaxation time. This is not the case since the simulations *in vacuo* provide an average relaxation time $\bar{T}_1$ for the amide I mode, which is quite similar to that obtained in the presence of the solvent (see Table III). These results are therefore consistent with the fact that at the initial stage, the amide I relaxation is dominated by IVR, with little contribution from the surrounding water molecules, in agreement with previous experimental[4] and theoretical[35] studies. We can conclude then that the low-frequency fourth, seventh, and eighth INMs, associated, respectively, with the δ(CNC) bending, amide IV and amide VI modes, along with their respective group *a* resonance modes, are basically responsible for the fast relaxation pathway of the amide I mode, acting as doorways to transfer the excess energy to the librations of the solvent.

More specifically we also see in Table III that the *in vacuo* simulations hardly change the fast relaxation time τ_1 but nearly double the slow relaxation time τ_2. This means that the solvent must certainly participate in the slow relaxation pathway. Since the direct VV transfer to the bending solvent modes is excluded in this respect, as previously discussed for the relaxation of the whole NMAD molecule, and as demonstrated now in Table III by the fact that the two amide I relaxation times do not change much when the solvent molecules are frozen, we arrive at the conclusion that the solvent participates in the slow amide I relaxation pathway through its librational motions in combination with two of the low-frequency modes of the solute so as to meet the energy transfer balance. It is interesting to note in this context that whereas the fast IVR relaxation proceeds through third order couplings, the slow relaxation channel would imply the simultaneous participation of four resonance modes, thus justifying the different time scales of these two relaxation pathways.

An additional test that can be made to verify the relaxation mechanisms of the amide I mode discussed above is to perform simulations with one of the low- frequency modes of the solute that participates in the fast relaxation pathway frozen. We have chosen for this purpose the seventh amide IV INM, which forms part of the pair of modes that best meets the resonance condition ($\bar{\omega}_{P\alpha\beta}$=4.3 cm^{-1}), and have accordingly carried out partially frozen simulations of the system with $\dot{Q}_7^e$=0, thus closing the channel that connects the amide I and amide IV modes. The short and long relaxation times obtained from these partially frozen simulations, also included in Table III, are τ_1=2.10 and τ_2=6.38 ps. They are both appreciably larger than the corresponding relaxation times extracted from the complete simulations 1.55 and 4.0 ps, respectively, thus corroborating the essential role that this mode plays in both relaxation pathways, as previously discussed. We also verified that the vibrational energy stored in the tenth INM remains practically unaffected by the freezing of the seventh amide IV ENM, as expected, since this mode does not exert any influence on the direct 2:1 resonance in which the tenth mode participates.

The results from our MD-INM simulations of the amide I vibrational relaxation of NMAD in liquid deuterated water can be rationalized using the three-stage kinetic model recently proposed by Dlott and co-workers[29,84,85] to account for the vibrational relaxation of medium-size biological molecules in solution. In this model, the vibrational modes of the solute molecule are classified in three tiers: the initially excited parent mode *P*, the midrange-energy modes *M*, and the lower- energy modes *L*. Typically, the midrange modes have energies in the 1200–1700 cm^{-1} range and the lower modes have energies below 1200 cm^{-1}. After initial excitation of the parent vibration, the population of this mode decays via IVR and its energy is transferred in the first stage to the midrange *M* and low-energy *L* vibrations, with little or no energy dissipated to the bath. In the second stage, the excited *M* vibrations decay by exciting *L* vibrations plus the bath and

the lower-energy vibrations decay by exciting the bath only. Finally, in the third stage, the remaining L excitations decay into the bath. As for the NMAD/$D_2O_{(l)}$ system, by identifying the parent vibration with the amide I mode, the midrange tier with the group a of modes, the lower-energy tier with the fourth, seventh, and eighth INMs, and the bath with the solvent librations, we find that the three-stage Dlott model describes quite well the main and fast relaxation pathway extracted from our nonequilibrium MD simulations.

To give numerical evidence of the efficiency of the Dlott model, we analyzed the variation in the vibrational energy content of the midrange M modes in the sequential kinetic scheme $P \rightarrow M+L \rightarrow L$, which is given by

$$\frac{E_i^{\mathrm{INM}}(t) - E_{i,\mathrm{eq}}^{\mathrm{INM}}}{E_i^{\mathrm{INM}}(0) - E_{i,\mathrm{eq}}^{\mathrm{INM}}} = k(e^{-t/\tau_{\mathrm{rel}}} - e^{-t/\tau_{\mathrm{exc}}}), \tag{20}$$

where τ_{exc} is the excitation time corresponding to the $P \rightarrow M+L$ step, τ_{rel} is the relaxation time for the $M+L \rightarrow L$ step, k is a parameter related to the maximum value of the energy content, and the subscript i denotes the specific midrange mode considered. In order to keep the number of fitting parameters to a minimum, we set $\tau_{\mathrm{exc}}=1.55$ ps, which is the value extracted from our simulations for the fast relaxation time of the amide I. The resulting fits are included in Fig. 5. As observed, the curves fitted reproduce our simulation results quite well. We find also that the relaxation time thus obtained for the tenth INM ($\tau_{\mathrm{rel}}=5.8$ ps) is substantially shorter than that derived for the a and b groups of modes ($\tau_{\mathrm{rel}}=10.7$ ps and $\tau_{\mathrm{rel}}=12.5$ ps, respectively). This is not surprising, since the frequency of the tenth INM is closer to those of the lower-energy L modes, which facilitates the vibrational relaxation. It is also noticeable that the relaxation times of the a and b groups of modes are similar to the relaxation time of the total vibrational energy of the NMAD molecule. This seems to indicate that this is the rate-determining step of the relaxation pathways.

Finally it is interesting to discuss our results in connection with those obtained by Fujisaki *et al.*[35,36,38] using different time-dependent perturbation schemes. These hybrid perturbation treatments show that the amide I mode relaxes mainly either through a combination of solute $M+L$ modes or through a 2:1 Fermi resonance, although the relative contributions of the different pathways vary substantially.[35,36,38] These findings are therefore in agreement with the results obtained from our nonequilibrium MD-INM simulations. However the existence should be noted by other studies on the relaxation of the amide I mode of the NMAD molecule in water clusters[51] and in liquid heavy water,[86,87] which report that the main relaxation channel is through the amide II mode, with the excess of energy being directly transferred to the solvent molecules.

IV. CONCLUSIONS

We performed nonequilibrium MD simulations of the vibrational relaxation dynamics of the NMAD amide I mode in liquid D_2O and used the INMs of the NMAD molecule to analyze the energy flows created by the relaxation of the amide I mode through the rest of the NMAD modes, and thus elucidate the relaxation mechanism that controls the whole process. The assignments of the INMs as they evolve over time, in terms of the ENMs, are made using the so-called min-cost algorithm originating from Economics and properly adapted to our problem, which provides a one-to-one relationship between both sets of modes. The INMs can thus be classified as pure or mixed depending on the magnitude of the couplings among the ENMs at a given time.

The vibrational decay of the amide I mode, initially excited in the $v=1$ state, is found to be biexponential, in agreement with previous experimental and theoretical studies, which implies that the relaxation proceeds through at least two mechanisms with different rate constants. A number of differently designed MD simulations have been carried out in order to understand the different aspects of the vibrational relaxation process, including simulations of the NMAD/$D_2O_{(l)}$ system with and without SHAKE to constrain the internal motions of the solvent molecules, simulations of the NMAD/$D_2O_{(l)}$ freezing a specific ENM, and *in vacuo* simulations of the NMAD molecule. We then comparatively analyzed the time evolution of the vibrational energy deposited in every INM of the NMAD molecule and, by calculating the time averaged vibrational frequencies of the INMs, we localized the main resonances that control the energy flows observed in the simulations.

As a result of the INM analysis of the MD simulations, we have found that the vibrational relaxation of the amide I mode is not statistical since not all the vibrations receive the same amount of energy, and that basically it proceeds through two different channels. The major, and faster, relaxation channel is associated with three main pathways involving combinations of the fourth, seventh, and eighth lower-frequency INMs with midrange-frequency modes. In addition, the tenth vibrational mode also receives a significant amount of energy from the amide I mode by a 2:1 resonance. This fast relaxation channel has been summarized by using a sequential kinetic mechanism of the type $P \rightarrow M+L \rightarrow L$, where the parent P is the initially excited normal mode, and M (*medium*) and L (*low*) are specific midrange- and lower-frequency vibrations, respectively. The minor, and slower, relaxation channel has been shown to be related to the participation of the librations of the solvent along with some low-frequency modes as the seventh INM. The use of MD simulations freezing one of the modes has been revealed as a particularly useful tool in this respect to elucidate the relaxation paths. These kinds of simulations can be performed in a straightforward way using the procedure described in this work. Furthermore, the role of the solvent during the vibrational relaxation has been discussed. While no significant VV energy transfer takes place between the NMAD normal modes and the bending D_2O modes, a fast vibrational energy transfer from the L modes to the rotational and translational motions of the solvent is observed.

Although the nonequilibrium MD-INM simulations of the NMAD/$D_2O_{(l)}$ system carried out in this work are in reasonable agreement with the measured data, a quantum description of the high frequency amide I mode is expected to be more realistic and to provide more accurate results. This suggests then the possibility of implementing hybrid

quantum/classical time-dependent simulations to describe the NMAD/$D_2O_{(l)}$ vibrational relaxation. Work along this line is currently in progress in our group.

ACKNOWLEDGMENTS

This work was partially supported by the Ministerio de Educación y Ciencia of Spain under Project Nos. CTQ2007-66528/BQU and CONSOLIDER CSD2009-00038, by the Fundación Séneca del Centro de Coordinación de la Investigación de la Región de Murcia under Project No. 08735/PI/08, by the Universidad Nacional de Quilmes, and by the CONICET. One of the authors (M.A.S.) acknowledges a fellowship provided by the Ministerio de Educación y Ciencia of Spain.

[1] A. Laubereau and W. Kaiser, Rev. Mod. Phys. **50**, 607 (1978).
[2] R. J. D. Miller, Annu. Rev. Phys. Chem. **42**, 581 (1991).
[3] Y. Mizutani and T. Kitagawa, Science **278**, 443 (1997).
[4] P. Hamm, M. H. Lim, and R. M. Hochstrasser, J. Phys. Chem. B **102**, 6123 (1998).
[5] D. Dlott, Chem. Phys. **266**, 149 (2001).
[6] M. T. Zanni, M. C. Asplund, and R. M. Hochstrasser, J. Chem. Phys. **114**, 4579 (2001).
[7] M. D. Fayer, Annu. Rev. Phys. Chem. **52**, 315 (2001).
[8] S. Woutersen and P. Hamm, J. Phys.: Condens. Matter **14**, R1035 (2002).
[9] A. M. Nagy, V. I. Prokhorenko, and R. J. D. Miller, Curr. Opin. Struct. Biol. **16**, 654 (2006).
[10] L. P. DeFlores, Z. Ganim, S. F. Ackley, H. S. Chung, and A. Tokmakoff, J. Phys. Chem. B **110**, 18973 (2006).
[11] Z. H. Wang, J. A. Carter, A. Lagutchev, Y. K. Koh, N.-H. Seong, D. G. Cahill, and D. D. Dlott, Science **317**, 787 (2007).
[12] P. Hamm, J. Helbing, and J. Bredenbeck, Annu. Rev. Phys. Chem. **59**, 291 (2008).
[13] S. Mukamel and R. Hochstrasser, Chem. Phys. **266**, 135 (2001).
[14] M. Lim, T. A. Jackson, and P. A. Anfinrud, Science **269**, 962 (1995).
[15] R. D. Vale and R. A. Milligan, Science **288**, 88 (2000).
[16] P. M. Felker and A. H. Zewail, Adv. Chem. Phys. **70**, 265 (1988).
[17] M. Kubo, E. Shiomitsu, K. Odai, T. Sugimoto, H. Suzuki, and E. Ito, J. Mol. Struct. **639**, 117 (2003).
[18] V. Pouthier, J. Chem. Phys. **128**, 065101 (2008).
[19] K. A. Peterson, C. W. Rella, J. R. Engholm, and H. A. Schwettman, J. Phys. Chem. B **103**, 557 (1999).
[20] A. Xie, L. van der Meer, W. Hoff, and R. Austin, Phys. Rev. Lett. **84**, 5435 (2000).
[21] R. Austin, A. Xie, L. van der Meer, B. Redlich, P. Lindgard, H. Frauenfelder, and D. Fu, Phys. Rev. Lett. **94**, 128101 (2005).
[22] M. Schade, A. Moretto, M. Crisma, C. Toniolo, and P. Hamm, J. Phys. Chem. B **113**, 13393 (2009).
[23] P. H. Nguyen, P. Derreumaux, and G. Stock, J. Phys. Chem. B **113**, 9340 (2009).
[24] P. H. Nguyen, S. Park, and G. Stock, J. Chem. Phys. **132**, 025102 (2010).
[25] S. Woutersen, Y. G. Mu, G. Stock, and P. Hamm, Proc. Natl. Acad. Sci. U.S.A. **98**, 11254 (2001).
[26] S. Woutersen, R. Pfister, P. Hamm, Y. Mu, D. S. Kosov, and G. Stock, J. Chem. Phys. **117**, 6833 (2002).
[27] I. V. Rubtsov, J. Wang, and R. M. Hochstrasser, J. Phys. Chem. A **107**, 3384 (2003).
[28] M. F. DeCamp, L. DeFlores, J. M. McCracken, A. Tokmakoff, K. Kwac, and M. Cho, J. Phys. Chem. B **109**, 11016 (2005).
[29] Y. Fang, S. Shigeto, N. Seong, and D. Dlott, J. Phys. Chem. A **113**, 75 (2009).
[30] S. K. Gregurick, G. M. Chaban, and R. B. Gerber, J. Phys. Chem. A **106**, 8696 (2002).
[31] P. H. Nguyen and G. Stock, J. Chem. Phys. **119**, 11350 (2003).
[32] K. Kwac and M. Cho, J. Chem. Phys. **119**, 2247 (2003).
[33] J. R. Schmidt, S. A. Corcelli, and J. L. Skinner, J. Chem. Phys. **121**, 8887 (2004).
[34] T. Hayashi, W. Zhuang, and S. Mukamel, J. Phys. Chem. A **109**, 9747 (2005).
[35] H. Fujisaki, Y. Zhang, and J. E. Straub, J. Chem. Phys. **124**, 144910 (2006).
[36] H. Fujisaki, K. Yagi, K. Hirao, and J. E. Straub, Chem. Phys. Lett. **443**, 6 (2007).
[37] H. Fujisaki and G. Stock, J. Chem. Phys. **129**, 134110 (2008).
[38] H. Fujisaki, K. Yagi, J. E. Straub, and G. Stock, Int. J. Quantum Chem. **109**, 2047 (2009).
[39] H. Fujisaki and J. E. Straub, J. Phys. Chem. B **111**, 12017 (2007).
[40] M. Bounouar and C. Scheurer, Chem. Phys. **323**, 87 (2006).
[41] A. L. Kaledin and J. M. Bowman, J. Phys. Chem. A **111**, 5593 (2007).
[42] W. D. Cornell, P. Cieplak, C. I. Bayly, I. R. Gould, J. K. M. Merz, D. M. Ferguson, D. C. Spellmeyer, T. Fox, J. W. Caldwell, and P. A. Kollman, J. Am. Chem. Soc. **117**, 5179 (1995).
[43] A. D. MacKerell, D. Bashford, M. Bellott, R. L. Dunbrack, J. D. Evanseck, M. J. Field, S. Fischer, J. Gao, H. Guo, S. Ha, D. Joseph-McCarthy, L. Kuchnir, K. Kuczera, F. T. K. Lau, C. Mattos, S. Michnick, T. Ngo, D. T. Nguyen, B. Prodhom, W. E. Reiher, III, B. Roux, M. Schlenkrich, J. C. Smith, R. Stote, J. Straub, M. Watanabe, J. Wiórkiewicz-Kuczera, D. Yin, and M. Karplus, J. Phys. Chem. B **102**, 3586 (1998).
[44] W. F. van Gunsteren *et al.*, J. Phys. Chem. A **103** (19), 3596 (1999).
[45] W. L. Jorgensen, D. S. Maxwell, and J. Tirado-Rives, J. Am. Chem. Soc. **118**, 11225 (1996).
[46] D. W. Oxtoby, Adv. Chem. Phys. **40**, 1 (1979).
[47] D. W. Oxtoby, Adv. Chem. Phys. **47**, 487 (1981).
[48] R. Rey and J. T. Hynes, J. Chem. Phys. **108**, 142 (1998).
[49] S. Li and W. H. Thompson, Chem. Phys. Lett. **405**, 304 (2005).
[50] D. E. Sagnella and J. E. Straub, Biophys. J. **77**, 70 (1999).
[51] Y. Zhang, H. Fujisaki, and J. E. Straub, J. Phys. Chem. A **113**, 3051 (2009).
[52] M. P. Allen and D. J. Tildesley, *Computer Simulations of Liquids* (Oxford Science, Oxford, 1987).
[53] V. S. Vikhrenko, C. Heidelbach, D. Schwarzer, V. B. Nemtsov, and J. Schroeder, J. Chem. Phys. **110**, 5273 (1999).
[54] G. Käb, C. Schröder, and D. Schwarzer, Phys. Chem. Chem. Phys. **4**, 271 (2002).
[55] M. Buchner, B. Ladanyi, and R. M. Stratt, J. Chem. Phys. **97**, 8522 (1992).
[56] T. Keyes, J. Phys. Chem. A **101**, 2921 (1997).
[57] R. M. Stratt, in *Ultrafast Infrared and Raman Spectroscopy*, edited by M. D. Fayer (Dekker, New York, 2001), pp. 149–190.
[58] X. G. Chen, R. Schweitzerstenner, S. Krimm, N. G. Mirkin, and S. A. Asher, J. Am. Chem. Soc. **116**, 11141 (1994).
[59] X. G. Chen, R. Schweitzerstenner, S. A. Asher, N. G. Mirkin, and S. Krimm, J. Phys. Chem. **99**, 3074 (1995).
[60] W. H. Miller, N. C. Handy, and J. E. Adams, J. Phys. Chem. **72**, 99 (1980).
[61] E. F. David and R. M. Stratt, J. Chem. Phys. **109**, 1375 (1998).
[62] K. Moritsugu and A. Kidera, J. Phys. Chem. B **108**, 3890 (2004).
[63] Y. Matsunaga, S. Fuchigami, and A. Kidera, J. Chem. Phys. **130**, 124104 (2009).
[64] G. Carpaneto, S. Martello, and P. Toth, Ann. Operat. Res. **13**, 193 (1988).
[65] M. Nakamura, K. Tamura, and S. Murakami, Thermochim. Acta **253**, 127 (1995).
[66] R. V. Pappu, R. K. Hart, and J. W. Ponder, J. Phys. Chem. B **102**, 9725 (1998).
[67] M. Svanberg, Mol. Phys. **92**, 1085 (1997).
[68] M. Rey-Lafon, M. T. Forel, and C. Garrigou-Lagrange, Spectrochim. Acta **29A**, 471 (1973).
[69] S. Ataka, H. Takeuchi, and M. Tasumi, J. Mol. Struct. **113**, 147 (1984).
[70] H. J. C. Berendsen, J. P. M. Postma, W. F. van Gunsteren, A. DiNola, and J. R. Haak, J. Chem. Phys. **81**, 3684 (1984).
[71] S. Park, P. H. Nguyen, and G. Stock, J. Chem. Phys. **131**, 184503 (2009).
[72] S. Y. Venyaminov and F. G. Prendergast, Anal. Biochem. **248**, 234 (1997).
[73] H. R. Zelsmann, J. Mol. Struct. **350**, 95 (1995).
[74] J. P. Ryckaert, G. Ciccotti, and H. J. C. Berendsen, J. Comput. Phys. **23**, 327 (1977).
[75] A. Bastida, C. Cruz, J. Zúñiga, A. Requena, and B. Miguel, J. Chem. Phys. **121**, 10611 (2004).
[76] A. Bastida, C. Cruz, J. Zúñiga, A. Requena, and B. Miguel, Chem. Phys. Lett. **417**, 53 (2006).

[77] A. Bastida, C. Cruz, J. Zúñiga, A. Requena, and B. Miguel, J. Chem. Phys. **126**, 014503 (2007).
[78] A. Bastida, J. Zuniga, A. Requena, and B. Miguel, J. Chem. Phys. **129**, 154501 (2008).
[79] A. Bastida, J. Zuniga, A. Requena, and B. Miguel, J. Chem. Phys. **131**, 204505 (2009).
[80] A. Bastida, M. Soler, J. Zúñiga, A. Requena, S. Fernández-Alberti, and A. Kalstein (unpublished).
[81] I. Ohmine and H. Tanaka, J. Chem. Phys. **93**, 8138 (1990).
[82] K. Moritsugu, O. Miyashita, and A. Kidera, Phys. Rev. Lett. **85**, 3970 (2000).
[83] K. Moritsugu, O. Miyashita, and A. Kidera, J. Phys. Chem. B **107**, 3309 (2003).
[84] S. Shigeto and D. D. Dlott, Chem. Phys. Lett. **447**, 134 (2007).
[85] S. Shigeto, Y. Pang, Y. Fang, and D. D. Dlott, J. Phys. Chem. B **112**, 232 (2008).
[86] A. G. Dijkstra, T. C. Jansen, R. Bloem, and J. Knoester, J. Chem. Phys. **127**, 194505 (2007).
[87] R. Bloem, A. G. Dijkstra, T. C. Jansen, and J. Knoester, J. Chem. Phys. **129**, 055101 (2008).